

Article

# Formation and Photoluminescence Properties of ZnO Nanoparticles on Electrospun Nanofibers Produced by Atomic Layer Deposition

Valerii Myndrul <sup>1,\*</sup>, Lucie Vysloužilová <sup>2</sup>, Andrea Klápšřová <sup>2</sup>, Emerson Coy <sup>1</sup> ,  
Mariusz Jancelewicz <sup>1</sup> and Igor Iatsunskyi <sup>1,\*</sup> 

<sup>1</sup> NanoBioMedical Centre, Adam Mickiewicz University, Wszechnicy Piastowskiej 3, 61-614 Poznan, Poland; coyeme@amu.edu.pl (E.C.); marjan7@amu.edu.pl (M.J.)

<sup>2</sup> Nanopharma, a.s., Nova 306, 530 09 Pardubice, Czech Republic; vyslouzilova@nanopharma.cz (L.V.); klapstova@nanopharma.cz (A.K.)

\* Correspondence: valmyn@amu.edu.pl (V.M.); igoyat@amu.edu.pl (I.I.)

Received: 17 November 2020; Accepted: 7 December 2020; Published: 9 December 2020



**Abstract:** The unique combination of optical, chemical, and structural properties of one-dimensional zinc oxide (1D ZnO) makes it one of the most attractive materials in a wide range of research and applications. In the present study, 1D ZnO nanomaterials were fabricated using a combination of two independent methods: electrospinning and atomic layer deposition (ALD). The electrospinning technique was used to produce 1D electrospun fibers consisting of four types of polymers: polylactic acid (PLLA), polyvinylidene fluoride (PVDF), polyvinyl alcohol (PVA), and polyamide 6 (PA6). The ALD technology, in turn, was selected as an excellent candidate for the synthesis of a ZnO thin layer over polymer fibers for the production of 1D ZnO/polymer nanofiber composites (PLLA/ZnO, PVDF/ZnO, PVA/ZnO, PA6/ZnO). Structural and optical properties of the produced nanofibers were studied by means of scanning electron microscopy (SEM), energy-dispersive X-ray spectroscopy (EDX), X-ray diffraction (XRD), diffuse reflectance, and photoluminescence (PL) spectroscopy. It was found that only PVDF/ZnO nanofibers exhibit stable room temperature PL that may be the result of a higher ZnO content in the sample. In addition, PL measurements were conducted as a function of excitation power and temperature in order to establish the main PL mechanisms and parameters for the PVDF/ZnO sample, as a most promising candidate for the biophotonic application.

**Keywords:** electrospinning; atomic layer deposition; polymers; photoluminescence

## 1. Introduction

One-dimensional (1D) ZnO nanomaterial is the object of the interest in a variety of studies due to its unique photoluminescent (PL) properties, high surface to volume ratio, biocompatibility, non-toxicity, and stability. Recently, 1D ZnO nanomaterials have been successfully utilized in sensors [1] and biosensor [2,3], energy applications [4,5], and purification [6], optoelectronics [7] and electronics [8], etc. 1D ZnO nanomaterials can be fabricated by the basic chemical methods based on bottom-up techniques, such as the vapor-solid (VS) process [9], vapor-liquid-solid (VLS) process [10], and top-down (lithographic techniques) [11]. Additionally, 1D ZnO nanocomposites can be produced by a combination of several independent techniques, such as electrospinning and atomic layer deposition (ALD). Among the various methods, electrospinning is a simple, controllable, and inexpensive method of making flexible polymer mats with uniform nanofiber lengths and diameters [12,13]. These attributes make polymer nanofibers ideal candidates for coating by a thin layer of ZnO, in order to obtain nanomaterials with the desired characteristics and properties. ALD is

an advanced and simple method for the deposition of thin metal oxide films over the substrates (both smooth and rough) [14]. This technique enables the production of highly conformal metal oxide (ZnO, TiO<sub>2</sub>, RuO<sub>2</sub>) layers on various surfaces for achieving high-quality compositions in comparison with other methods [15–17]. Thus, ALD is an excellent technique to deposit a thin metal oxide layer on polymer nanofibers, with the ability to adjust the electronic and optical properties of the produced nanocomposites [3]. Recently, it was demonstrated that different 1D ZnO nanocomposites and other 1D nanomaterials can be synthesized by using both of those techniques [18–20]. It was shown that the most promising 1D nanocomposites were produced from polyacrylonitrile (PAN) covered by ZnO [3,12,18]. However, it is still an “open question” about the application of other electrospun polymers for the production of 1D ZnO-polymer nanofibers.

Electrospinning can be used for both water-soluble and water-resistant polymers. However, only a limited number of polymers can be electrospun from aqueous solutions, i.e., polyethylene oxide (PEO) and polyvinyl alcohol (PVA) [21]. Among the water-resistant polymers, the most popular are polyacrylonitrile (PAN), polylactic acid (PLLA), polyvinylidene fluoride (PVDF), and polyamide 6 (PA6), etc. Nanofibers produced from those polymers are used in a large number of applications and products, such as tissue engineering [22], filtration [23], scaffolding [24], sensors [25] and biosensors [26], water purification [27], direct contact membrane distillation [28], hemostasis [29], VLC technology [30], energy harvesting [31], etc. Furthermore, nanofibers seem to be attractive for wound dressing [32] and anti-tumor therapy [33] due to the excellent biocompatibility and low toxicity. Despite the fact that pure electrospun polymers are already well-studied, nanocomposites based on polymer nanofibers still remain within the scope of scientific interest. For example, nanocomposites made of polymer fibers and metal/metal oxide nanoparticles or nanolayers can be attractive for optics, electronics, and magnetism.

In present work, we report on the investigation of the structural and optical properties of four different electrospun polymer (PVA, PA6, PVDF, PLLA) nanofibers covered by the ALD ZnO. The morphology and structural properties of the nanofibers were characterized by X-ray diffraction analysis (XRD), and scanning electron microscopy (SEM) combined with an energy dispersive X-ray spectroscopy (EDX) analysis. The optical properties of PVA, PA6, PVDF, PLLA, and PVA/ZnO, PA6/ZnO, PVDF/ZnO, PLLA/ZnO nanofibers were investigated by diffuse reflectance and photoluminescence (PL). For PVDF/ZnO nanofibers, the dependence of the PL vs. the excitation power and the temperature are studied. This is the first research where different types of polymer fibers were used for ZnO ALD deposition.

## 2. Materials and Methods

### 2.1. Samples Production

Samples were produced by the two-step procedure: (i) electrospinning; and (ii) ALD. At the beginning, four different polymers were used in order to produce nanofibers (see Table 1). Taking into account the temperature of the ALD process (around 120 °C), the melting temperature of polymers should be higher than this value. Electrospinning was performed for the prepared polymer solutions. Polymer solution was delivered through a needleless spinning electrode and was subjected to a strong electric field. The polymer solution was then drawn and elongated by external and internal electric forces, and nanofibers were created. Nanospider™ (NS 1WS500U, Elmarco, Liberec, Czech Republic) was used for electrospinning of prepared polymer solutions. The climatic conditions were controlled by a precisely controlled air conditioning system (NS AC150 (Elmarco)). The distance between the spinning electrode and the counter-electrode (collector) was tuned for each polymer. The cartridge speed was 200 mm/s, the rewinding speed of the substrate to collect nanofibers (Spunbond, Pegas Nonwovens, Znojmo, Czech Republic) was 10 mm/min. The temperature was 23 °C and the relative humidity was 40%.

**Table 1.** Electrospun nanofibers.

Full Name	Short Name	Parameters and Specification
Polyvinylidene fluoride	PVDF	Sigma Aldrich, Mw: 180,000 g/mol, melting temperature ca. 170 °C
Polyamid 6	PA6	Ultradid, Mw: 66,000 g/mol, melting temperature ca. 215 °C
Polylactic acid	PLLA	Sigma Aldrich, Mw: 60,000 g/mol, melting temperature ca. 170 °C
Polyvinyl alcohol	PVA	Sigma Aldrich, Mw: 130,000 g/mol, melting temperature ca. 200 °C

A commercially available Picosun ALD reactor (Masala, Finland) was used for the deposition of ZnO. The deposition process used diethyl zinc (DEZ) and deionized water as precursors, which reacted at 120 °C and yielded a thickness of 2.1 Å per one ALD cycle (corresponding to a flat surface). The number of ALD cycles was varied as 100 and 200, corresponding to a layer thickness of 20 nm and 40 nm, respectively. After every cycle, the reactor chamber was purged by an intense N<sub>2</sub> flow in order to remove the byproducts of the chemical reactions. Taking into account that 100 ALD cycles did not lead to the formation of crystalline ZnO, only samples with 200 ALD cycles were considered for further discussion.

## 2.2. Characterization

The structural properties of PSi/ZnO nanocomposites were analyzed by a JEOL JSM 7001F (Tokyo, Japan) SEM equipped with an EDX analyzer (JEOL, Tokyo, Japan). The XRD measurements were performed by X'pert3 MRD (XL) from a PANalytical Cu K $\alpha$  radiation source (wavelength of 1.54 Å) and operating at 45 kV and 40 mA (Almelo, The Netherlands).

The diffuse reflectance measurements of PSi/ZnO nanocomposites were performed on an Ocean Optics QE PRO fiber optic spectrometer (Ostfildern, Germany) combined with an integrating sphere and a Xe light source. Acquisition of PL data was performed using a He-Cd laser from Kimmon Koha (Tokyo, Japan) with a wavelength of 325 nm and the emission spectra were recorded in the range from 360 to 900 nm by an Ocean Optics USB4000 spectrometer (Dunedin, FL, USA). Analysis of PL vs. temperature was performed using Linkam thms 600 stage in the range of 83 to 443° K. The PL power-dependence measurements were performed by using neutral density filters to achieve different excitation powers varying between 0.05 and 8 mW (calibrated by a Thorlabs S120VC Si photodiode (Jessup, MD, USA)).

## 3. Results and Discussion

### 3.1. Structural Characterization

In order to investigate the morphology and structural properties of the fabricated nanocomposites, SEM, EDX, XRD were performed and discussed. Figure 1 represents the surface morphology of each polymer nanofibers as well as their nanocomposites with ZnO. Figure 1a,e are the top-view images of PVA and PVA/ZnO composites, respectively. There is no significant difference between the nanofibers structure before and after the ALD process. The average fiber diameter is around 200 nm for both samples. Furthermore, EDX analysis (inset tables) indicates the presence of ZnO inclusions inside/over the nanofibers structure for the PVA/ZnO sample. Figure 1b,f represent the morphologies of PA6 and PA6/ZnO nanofibers with average diameters around 150 nm. No visible changes observed for the nanofiber structures before and after the ALD process. EDX analysis indicates the presence of ZnO inclusions within the PA6 fiber matrix. Figure 1c,g exhibit the surface morphologies of PVDF and PVDF/ZnO nanofibers, respectively. It can be stated that the morphologies of pure PVDF and PVDF/ZnO nanofibers are similar, and the average fiber diameter was evaluated as 150 nm. The EDX analysis of this sample indicates the presence of ZnO in the matrix of PVDF fibers. The PLLA and PLLA/ZnO nanofibers with average diameters 200 nm are shown in the Figure 1d,h,

respectively. The EDX measurement confirms that the ZnO inclusions are within the fiber matrix after the ALD process.

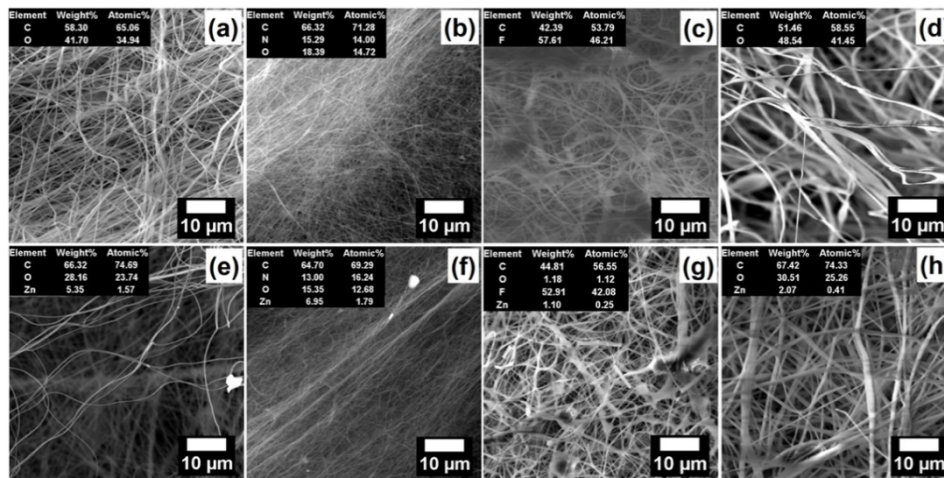


**Figure 1.** SEM images of the top view of PVA (a), PA6 (b), PVDF (c), PLLA (d), PVA/ZnO (e), PA6/ZnO (f), PVDF/ZnO (g), PLLA/ZnO (h) nanofibers. Inset tables are EDX measurements for each sample.

Figure 2a–d represents the high-resolution SEM images of PVA/ZnO, PA6/ZnO, PVDF/ZnO, and PLLA/ZnO nanofibers, respectively. It can be noted that the ZnO coats the fiber's surface heterogeneously for all samples, which is abnormal for the ALD process as it can provide homogeneous ZnO coating in ZnO/polymer fiber structures. This might be explained by heterogeneously-distributed -OH groups, which are centers of the DEZ precursor adsorption during ALD, over the surface of the fibers. We may assume that an additional chemical treatment (functionalization) should be performed before ALD in order to achieve the homogeneous coverage of nanofibers by ALD. Our previous research demonstrated that PAN polymers are covered by the conformal ALD ZnO without any functionalization procedures [3,12,18].

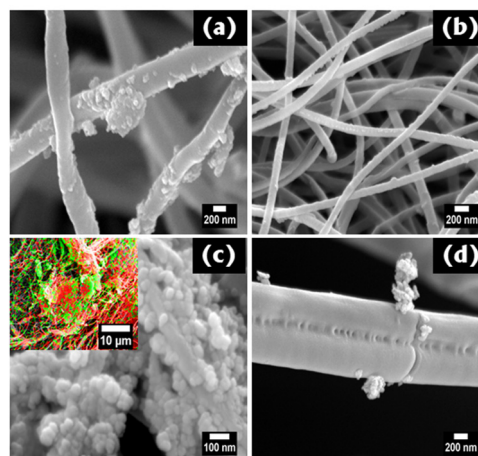


**Figure 2.** HR-SEM images of (a) PVA/ZnO, (b) PA6/ZnO, (c) PVDF/ZnO, and (d) PLLA/ZnO nanofibers. Inset image is the EDX mapping of PVDF/ZnO nanofiber. (green—Zn; red—C).

HR-SEM also demonstrates that ZnO nanoparticles are different from sample to sample, and their diameters vary from 10 to 50 nm for the PVA/ZnO, PVDF/ZnO, and PLLA/ZnO samples while, for the PA6/ZnO sample, ZnO nanoparticles are no more than 20 nm in diameter. More attention should be paid to the PVDF/ZnO sample due to its significant coverage by ZnO nanocrystallites, which is confirmed by the SEM images (Figure 2c) and EDX mapping (green areas on the inset image). The average ZnO

crystallite diameter can be estimated as 50 nm. The clusters of ZnO nanoparticles can reach 1–5  $\mu\text{m}$  in diameter. To summarize the information obtained from the SEM and EDX measurements, one can note that the ALD process did not provide homogenous ZnO coating and formation of the ZnO/polymer nanofiber core/shell structure.

In order to confirm the crystalline phase of ZnO of fabricated samples (PVA/ZnO, PA6/ZnO, PVDF/ZnO, PLLA/ZnO), XRD measurements were performed and analyzed (Figure 3). It is clearly seen that the crystallinity of ZnO is inherent only to the PVDF/ZnO and PVA/ZnO nanofibers, which is in good agreement with the above-reported high-resolution SEM investigations. Peaks (sample PVDF/ZnO) at  $2\theta = 9.32^\circ, 18.73^\circ, 20.5^\circ$  correspond to the PVDF polymer, while peaks at  $2\theta = 31.59^\circ, 34.40^\circ,$  and  $36.13^\circ$  indicate the ZnO wurtzite structure. The PVA/ZnO sample indicates the similar behavior, where along with PVA polymer peaks ( $2\theta = 7.18^\circ, 19.46^\circ$ ) one can observe wurtzite ZnO peaks at  $2\theta = 31.59^\circ, 34.40^\circ,$  and  $36.13^\circ, 47.54^\circ, 56.60^\circ$ . The average crystalline size for both PVDF/ZnO and PVA/ZnO nanofibers was calculated by the Debye–Scherrer equation (Equation (1)) and estimated as  $7 \pm 2$  nm. The remaining two samples (PA6/ZnO and PLLA/ZnO) exhibit amorphous phase of ZnO.

$$D = \frac{0.9 \times \lambda}{\beta \times \cos(\theta)} \quad (1)$$

where  $\beta$ ,  $\theta$ , and  $\lambda$  are full width of half maximum, diffraction angle, and X-ray wavelength ( $\lambda = 0.154$  nm), respectively.

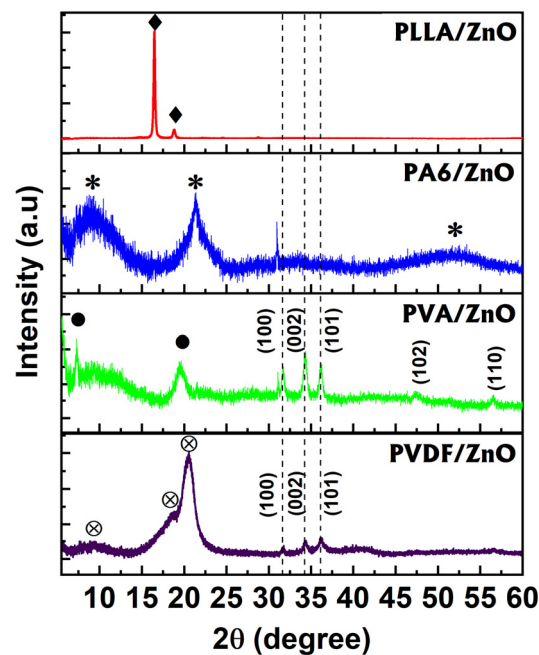


**Figure 3.** XRD patterns of the PVDF/ZnO, PVA/ZnO, PA6/ZnO, and PLLA/ZnO nanofibers (symbols: black rhomb—PLLA, stars—PA6, black circles—PVA and crossed circles—PVDF; dot lines—ZnO).

### 3.2. Optical Properties

Diffuse reflectance measurements were applied in order to analyze the absorbance properties of obtained 1D ZnO/polymer nanofibers by using Kubelka–Munk method [15]. The UV–VIS–NIR absorption spectra at room temperature were investigated to estimate the band gap changes before and after the ALD process. The band gaps were calculated by using the Tauc equation (Equation (2)) for direct band gap semiconductors:

$$(ah\nu)^2 = C(h\nu - E_g) \quad (2)$$

where  $\alpha$  is the optical absorption coefficient,  $h\nu$  is the incident photon energy, and  $C$  is a constant. The band gaps ( $E_g$ ) were determined by plotting  $(\alpha h\nu)^2$  vs  $h\nu$  and extrapolating the linear absorption edge of the curve to intersect the energy axis.

It is clearly seen that there are no significant changes for PA6 and ZnO/PA6 samples (Figure 4c). Taking into account the analysis of the electron microscopy and the XRD, one may assume that PA6 fibers have not been covered by ALD ZnO or covered by a small amount of ZnO. The band gap value for PVA is around 3.7 eV. After ZnO deposition, one may observe a small shift to 3.68 eV (Figure 4b). For PLLA and PLLA/ZnO samples, the perceptible band gap change from 4.15 to 3.69 eV can be seen (Figure 4a). Such a behavior of the band gap shift can be explained by the embedding of ZnO (probably amorphous or highly crystalline phase) into the PLLA nanofibers matrix. A similar behavior is observed for the PVDF and PVDF/ZnO nanofibers (Figure 4d). The observable band gap shift from 4.18 eV (PVDF nanofibers) to 3.7 eV (PVDF/ZnO) indicates the presence of some ZnO inclusions/nanoparticles into the PVDF nanofibers matrix. The band gap value of ZnO for samples (PLLA/ZnO, PVA/ZnO, and PVDF/ZnO) are calculated to be around 3.7 eV, which is higher than the previously reported values for ZnO micro- and nanoparticles 3.4–3.6 eV [34,35]. The increase of the band gap value might be explained by the quantum confinement effect [15].

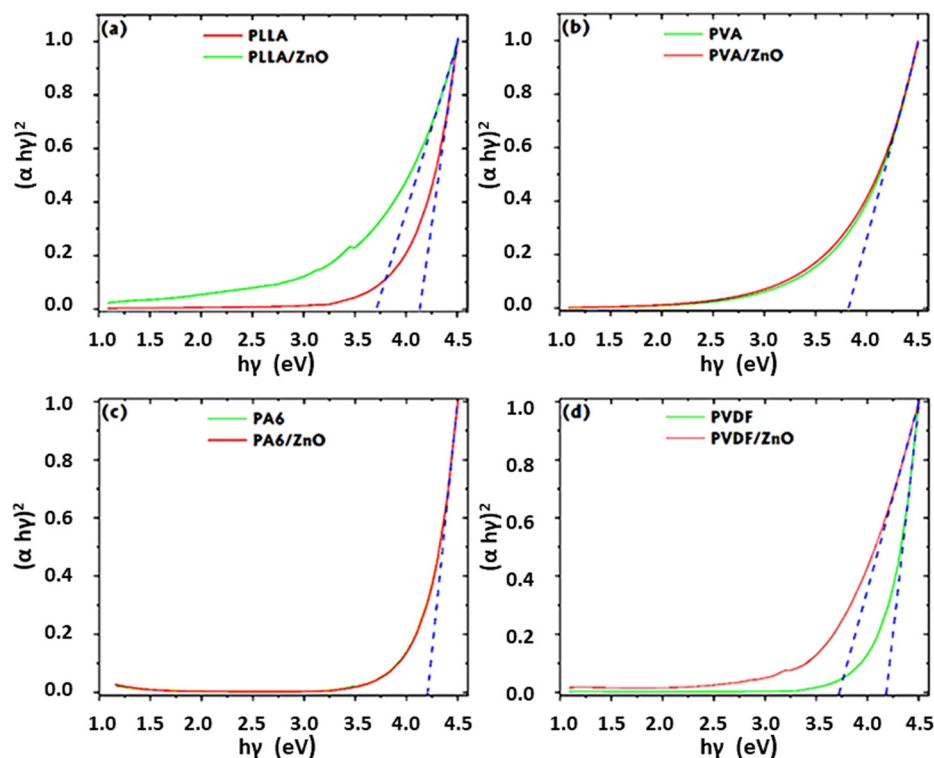


**Figure 4.** Tauc plots of (a) the PLLA and PLLA/ZnO nanofibers, (b) PVA and PVA/ZnO nanofibers, (c) PA6 and PA6/ZnO nanofibers, (d) PVDF and PVDF/ZnO nanofibers.

Room-temperature (RT) PL spectra of pure PVA, PLLA, PA6, PVDF, and PVA/ZnO, PLLA/ZnO, PA6/ZnO, PVDF/ZnO in the wavelength range of 340 to 900 nm are shown in Figure 5a,b. Figure 5a indicates that almost nanofibers demonstrate the same PL spectra, which is associated with the light scattering and emission from the substrate. This confirms the irregular ZnO coating over the polymer fibers and low ZnO concentration within the fibers. On the other hand, the PVDF/ZnO fibers showed a different PL spectrum with a broad visible emission (PL peak at around 540 nm). The PVDF/ZnO emission in the visible region is significantly different from the emission of pure PVDF and other samples (Figure 5b) and is associated with the defect-related emissions of ZnO nanoparticles [35]. Those defect states in ZnO nanostructures can be divided into two groups: (i) shallow trapped states,

which are located near the conductive band (CB), consisted of optically active zinc-related intrinsic defect states such as zinc interstitials ( $Zn_i$ ) and zinc vacancies ( $V_{Zn}$ ), and (ii) deep trapped defect states, such as oxygen vacancy ( $V_O$ ), oxygen interstitial ( $O_i$ ), and oxygen at zinc lattice site ( $O_{Zn}$ ) [3,12].

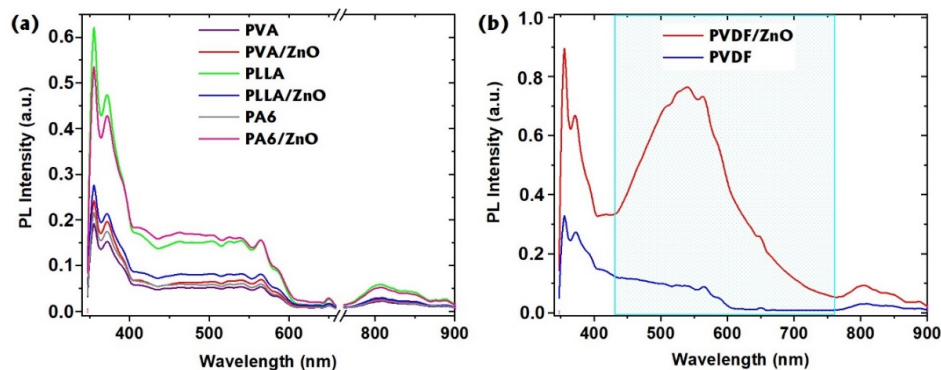


**Figure 5.** Room temperature PL of the pristine polymers nanofibers and (a) PVA/ZnO, PA6/ZnO, and PLLA/ZnO nanofibers; and (b) PVDF/ZnO ( $\lambda_{excitation} = 325$  nm).

### 3.3. Photoluminescence Analysis of PVDF/ZnO Nanofibers

Based on the analysis of structural and optical properties of produced 1D ZnO nanofibers, we concluded that the most promising nanocomposite for photonic and/or biosensing applications could be PVDF/ZnO nanofibers. Additionally, those fibers could be used for piezoelectric applications because both materials can generate electrical potential under mechanical deformations [36,37]. In order to study the mechanisms of PL emission in PVDF/ZnO nanofibers additional measurements (PL vs. the temperature and the excitation power) were performed.

RT PL spectra of PVDF/ZnO nanofibers excited by He-Cd laser at different energies are shown in Figure 6a. As the excitation energy increases, the intensity of the defect emission (peak at 540 nm) becomes stronger. The PL peak position and width of the band do not show a noticeable change. The room temperature PL intensity of defect emission is plotted against the excitation power in Figure 6b. It is well-known that the PL intensity depends on the excitation power ( $P$ ) as [12]:

$$I \sim P^k \quad (3)$$

where  $k$  is the power coefficient. Calculated values of the power coefficient are around 1 confirming the donor-acceptor defects emissions from ZnO nanoparticles [38].

Temperature-dependent PL measurements provide valuable information on the quenching of the emission. The PL spectra of PVDF/ZnO nanofibers were measured in a temperature range of 83–443 K as shown in Figure 6c. The increase of the temperature leads to the decrease of the PL intensity. Additionally, one may observe the small shift of the PL peak position that is explained by electron–phonon interactions [35]. We also observed the drop of PL intensity at 420 K that can be explained by melting of the polymer fiber, and as consequence, structural changes of 1D ZnO/PVDF nanofibers took place. This value of the temperature determines the critical point of the fibers application.

It is well-known that the quenching of the PL intensity ( $I$ ) can be described by the following equation [35]:

$$I \sim \frac{1}{1 + C \times \exp\left(\frac{E_A}{kT}\right)} \quad (4)$$

where  $E_A$  is the activation energy, and  $k$ ,  $C$ , and  $T$  are the Boltzmann constant, proportional coefficient, and absolute temperature, respectively. The obtained dependences  $I(T)$  were plotted in semi-logarithmic scale and then fitted by an exponential function (Figure 6b) to calculate activation energies. One can observe two slopes of the line meaning two different activation energies can be estimated. The values

of the  $E_A$  for 1D PVDF/ZnO nanofibers were found to be 0.032 and 0.37 eV. Those values of  $E_A$  correlate with similar values detected for ZnO nanostructures and corresponds to energetic distances between radiative and nonradiative transitions [35,39]. The values of activation energy correspond to bulk (0.37 eV) and surface (0.032 eV) nonradiative defects.

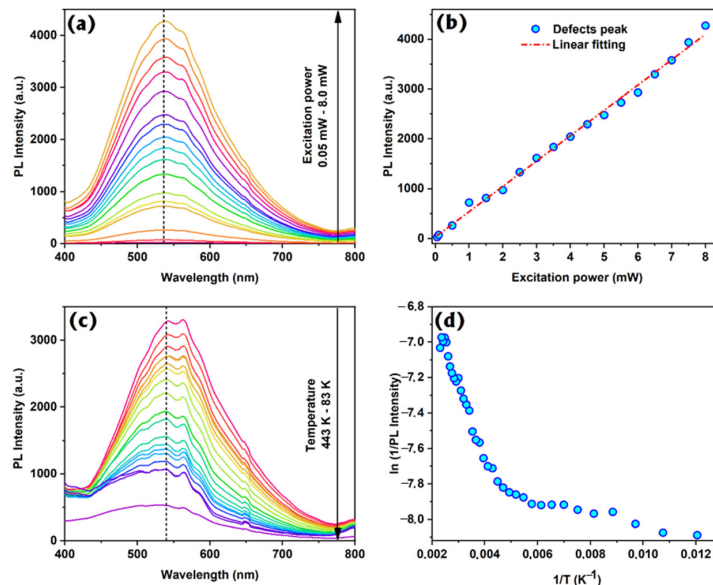


**Figure 6.** (a) PL power-dependence spectra and (b) the peak position vs. excitation power; (c) PL temperature dependence; and (d) logarithmic approximation for the PVDF/ZnO sample.

#### 4. Conclusions

In summary, 1D ZnO-polymer (PVDF, PLLA, PVA, PA6) nanofibers were fabricated using electrospinning and ALD techniques. Their structural and optical properties were determined. It is demonstrated that polymer fibers are covered by ZnO heterogeneously, and ZnO is presented in the form of nanoparticles with an average size of 7 nm (for PVDF/ZnO and PVA/ZnO samples). Comparing the proposed results with our previous experiments with ZnO/PAN nanofibers, one may conclude that an additional chemical treatment of nanofibers should be performed in order to produce a conformal ZnO layer over the whole surface of the polymer. The most promising PL properties demonstrate ZnO/PVDF nanofibers. The mechanisms of PL and activation energies for ZnO/PVDF nanofibers were established.

**Author Contributions:** Conceptualization: I.I.; methodology: I.I.; sample fabrication: L.V., A.K., M.J., and I.I.; investigations: E.C., V.M. and I.I.; interpretation of data: V.M. and I.I.; writing—original draft preparation: V.M. and I.I.; writing—review and editing: I.I.; drafting the work: V.M.; supervision: I.I.; project administration: I.I.; funding acquisition: I.I. All authors have read and agreed to the published version of the manuscript.

**Funding:** Authors acknowledge the financial support by project H2020-MSCA-RISE-2017, ‘Novel 1D photonic metal oxide nanostructures for early stage cancer detection’ (Project number: 778157). V.M. acknowledges the partial financial support from the project ‘‘Środowiskowe interdyscyplinarne studia doktoranckie w zakresie nanotechnologii’’ no. POWR.03.02.00-00-I032/16 under the European Social Fund—Operational Programme Knowledge Education Development, Axis III Higher Education for Economy and Development, Action 3.2 PhD Programme. V.M. acknowledges the partial financial support from OPUS 14 project 2017/27/B/ST8/01506 financed by the National Science Center of Poland.

**Conflicts of Interest:** The authors declare no conflict of interest.

#### References

1. Barreca, D.; Bekermann, D.; Comini, E.; Devi, A.; Fischer, R.A.; Gasparotto, A.; MacCato, C.; Sberveglieri, G.; Tondello, E. 1D ZnO nano-assemblies by Plasma-CVD as chemical sensors for flammable and toxic gases. *Sens. Actuators B Chem.* **2010**, *149*, 1–7. [[CrossRef](#)]

2. Viter, R.; Savchuk, M.; Starodub, N.; Balevicius, Z.; Tumenas, S.; Ramanaviciene, A.; Jevdokimovs, D.; Erts, D.; Iatsunskiy, I.; Ramanavicius, A. Photoluminescence immunosensor based on bovine leukemia virus proteins immobilized on the ZnO nanorods. *Sens. Actuators B Chem.* **2019**, *285*, 601–606. [[CrossRef](#)]
3. Myndrul, V.; Coy, E.; Bechelany, M.; Iatsunskiy, I. Photoluminescence label-free immunosensor for the detection of Aflatoxin B1 using polyacrylonitrile/zinc oxide nanofibers. *Mater. Sci. Eng. C* **2021**, *118*, 111401. [[CrossRef](#)]
4. Wang, M.; Ren, F.; Zhou, J.; Cai, G.; Cai, L.; Hu, Y.; Wang, D.; Liu, Y.; Guo, L.; Shen, S. N Doping to ZnO Nanorods for Photoelectrochemical Water Splitting under Visible Light: Engineered Impurity Distribution and Terraced Band Structure. *Sci. Rep.* **2015**, *5*, 12925. [[CrossRef](#)] [[PubMed](#)]
5. Pavlenko, M.; Siuzdak, K.; Coy, E.; Załęski, K.; Jancelewicz, M.; Iatsunskiy, I. Enhanced solar-driven water splitting of 1D core-shell Si/TiO<sub>2</sub>/ZnO nanopillars. *Int. J. Hydrogen Energy* **2020**, *45*, 26426–26433. [[CrossRef](#)]
6. Ishikawa, Y.; Shimizu, Y.; Sasaki, T.; Koshizaki, N. Preparation of zinc oxide nanorods using pulsed laser ablation in water media at high temperature. *J. Colloid Interface Sci.* **2006**, *300*, 612–615. [[CrossRef](#)] [[PubMed](#)]
7. Panda, D.; Tseng, T.-Y. One-dimensional ZnO nanostructures: Fabrication, optoelectronic properties, and device applications. *J. Mater. Sci.* **2013**, *48*, 6849–6877. [[CrossRef](#)]
8. Senthilkumar, N.; Vivek, E.; Shankar, M.; Meena, M.; Vimalan, M.; Potheher, I.V. Synthesis of ZnO nanorods by one step microwave-assisted hydrothermal route for electronic device applications. *J. Mater. Sci. Mater. Electron.* **2018**, *29*, 2927–2938. [[CrossRef](#)]
9. Umar, A.; Kim, S.H.; Lee, Y.S.; Nahm, K.S.; Hahn, Y.B. Catalyst-free large-quantity synthesis of ZnO nanorods by a vapor-solid growth mechanism: Structural and optical properties. *J. Cryst. Growth* **2005**, *282*, 131–136. [[CrossRef](#)]
10. Wang, X.; Summers, C.J.; Wang, Z.L. Large-Scale Hexagonal-Patterned Growth of Aligned ZnO Nanorods for Nano-optoelectronics and Nanosensor Arrays. *Nano Lett.* **2004**, *4*, 423–426. [[CrossRef](#)] [[PubMed](#)]
11. Ahsanulhaq, Q.; Kim, J.-H.; Hahn, Y.-B. Controlled selective growth of ZnO nanorod arrays and their field emission properties. *Nanotechnology* **2007**, *18*, 485307. [[CrossRef](#)]
12. Damberga, D.; Viter, R.; Fedorenko, V.; Iatsunskiy, I.; Coy, E.; Graniel, O.; Balme, S.; Miele, P.; Bechelany, M. Photoluminescence Study of Defects in ZnO-Coated Polyacrylonitrile Nanofibers. *J. Phys. Chem. C* **2020**, *124*, 9434–9441. [[CrossRef](#)]
13. Blachowicz, T.; Ehrmann, A. Recent developments in electrospun ZnO nanofibers: A short review. *J. Eng. Fibers Fabr.* **2020**, *15*, 155892501989968. [[CrossRef](#)]
14. Pavlenko, M.; Myndrul, V.; Gottardi, G.; Coy, E.; Jancelewicz, M.; Iatsunskiy, I. Porous Silicon-Zinc Oxide Nanocomposites Prepared by Atomic Layer Deposition for Biophotonic Applications. *Materials* **2020**, *13*, 1987. [[CrossRef](#)] [[PubMed](#)]
15. Brytavskiy, I.; Hušeková, K.; Myndrul, V.; Pavlenko, M.; Coy, E.; Zaleski, K.; Gregušová, D.; Yate, L.; Smyntyna, V.; Iatsunskiy, I. Effect of porous silicon substrate on structural, mechanical and optical properties of MOCVD and ALD ruthenium oxide nanolayers. *Appl. Surf. Sci.* **2019**, *471*, 686–693. [[CrossRef](#)]
16. Graniel, O.; Fedorenko, V.; Viter, R.; Iatsunskiy, I.; Nowaczyk, G.; Weber, M.; Załęski, K.; Jurga, S.; Smyntyna, V.; Miele, P.; et al. Optical properties of ZnO deposited by atomic layer deposition (ALD) on Si nanowires. *Mater. Sci. Eng. B* **2018**, *236–237*, 139–146. [[CrossRef](#)]
17. Pavlenko, M.; Coy, E.L.; Jancelewicz, M.; Załęski, K.; Smyntyna, V.; Jurga, S.; Iatsunskiy, I. Enhancement of optical and mechanical properties of Si nanopillars by ALD TiO<sub>2</sub> coating. *RSC Adv.* **2016**, *6*, 97070–97076. [[CrossRef](#)]
18. Iatsunskiy, I.; Vasylenko, A.; Viter, R.; Kempirski, M.; Nowaczyk, G.; Jurga, S.; Bechelany, M. Tailoring of the electronic properties of ZnO-polyacrylonitrile nanofibers: Experiment and theory. *Appl. Surf. Sci.* **2017**, *411*, 494–501. [[CrossRef](#)]
19. Coy, E.; Siuzdak, K.; Pavlenko, M.; Załęski, K.; Graniel, O.; Ziótek, M.; Balme, S.; Miele, P.; Weber, M.; Bechelany, M.; et al. Enhancing photocatalytic performance and solar absorption by schottky nanodiodes heterojunctions in mechanically resilient palladium coated TiO<sub>2</sub>/Si nanopillars by atomic layer deposition. *Chem. Eng. J.* **2020**, *392*, 123702. [[CrossRef](#)]
20. Barhoum, A.; El-Maghrabi, H.H.; Iatsunskiy, I.; Coy, E.; Renard, A.; Salameh, C.; Weber, M.; Sayegh, S.; Nada, A.A.; Roualdes, S.; et al. Atomic layer deposition of Pd nanoparticles on self-supported carbon-Ni/NiO-Pd nanofiber electrodes for electrochemical hydrogen and oxygen evolution reactions. *J. Colloid Interface Sci.* **2020**, *569*, 286–297. [[CrossRef](#)]
21. Jin, H.-J.; Fridrikh, S.V.; Rutledge, G.C.; Kaplan, D.L. Electrospinning Bombyx mori Silk with Poly(ethylene oxide). *Biomacromolecules* **2002**, *3*, 1233–1239. [[CrossRef](#)] [[PubMed](#)]

22. Nagarajan, S.; Belaid, H.; Pochat-Bohatier, C.; Teyssier, C.; Iatsunskyi, I.; Coy, E.; Balme, S.; Cornu, D.; Miele, P.; Kalkura, N.S.; et al. Design of Boron Nitride/Gelatin Electrospun Nanofibers for Bone Tissue Engineering. *ACS Appl. Mater. Interfaces* **2017**, *9*, 33695–33706. [[CrossRef](#)] [[PubMed](#)]
23. Zhang, S.; Tang, N.; Cao, L.; Yin, X.; Yu, J.; Ding, B. Highly Integrated Polysulfone/Polyacrylonitrile/Polyamide-6 Air Filter for Multilevel Physical Sieving Airborne Particles. *ACS Appl. Mater. Interfaces* **2016**, *8*, 29062–29072. [[CrossRef](#)] [[PubMed](#)]
24. Abdal-hay, A.; Hussein, K.H.; Casettari, L.; Khalil, K.A.; Hamdy, A.S. Fabrication of novel high performance ductile poly(lactic acid) nanofiber scaffold coated with poly(vinyl alcohol) for tissue engineering applications. *Mater. Sci. Eng. C* **2016**, *60*, 143–150. [[CrossRef](#)]
25. Liu, N.; Fang, G.; Wan, J.; Zhou, H.; Long, H.; Zhao, X. Electrospun PEDOT:PSS–PVA nanofiber based ultrahigh-strain sensors with controllable electrical conductivity. *J. Mater. Chem.* **2011**, *21*, 18962. [[CrossRef](#)]
26. Sapountzi, E.; Chateaux, J.-F.; Lagarde, F. Combining Electrospinning and Vapor-Phase Polymerization for the Production of Polyacrylonitrile/ Polypyrrole Core-Shell Nanofibers and Glucose Biosensor Application. *Front. Chem.* **2020**, *8*, 678. [[CrossRef](#)]
27. Bai, L.; Jia, L.; Yan, Z.; Liu, Z.; Liu, Y. Plasma-etched electrospun nanofiber membrane as adsorbent for dye removal. *Chem. Eng. Res. Des.* **2018**, *132*, 445–451. [[CrossRef](#)]
28. Liao, Y.; Wang, R.; Tian, M.; Qiu, C.; Fane, A.G. Fabrication of polyvinylidene fluoride (PVDF) nanofiber membranes by electro-spinning for direct contact membrane distillation. *J. Membr. Sci.* **2013**, 30–39. [[CrossRef](#)]
29. Bera, B. Preparation of Polymer Nanofiber and Its Application. *Asian J. Phys. Chem. Sci.* **2017**, *2*, 1–4. [[CrossRef](#)]
30. Dadabayev, R.; Malka, D. A visible light RGB wavelength demultiplexer based on polycarbonate multicore polymer optical fiber. *Opt. Laser Technol.* **2019**, *116*, 239–245. [[CrossRef](#)]
31. Mansouri, S.; Sheikholeslami, T.F.; Behzadmehr, A. Investigation on the electrospun PVDF/NP-ZnO nanofibers for application in environmental energy harvesting. *J. Mater. Res. Technol.* **2019**, *8*, 1608–1615. [[CrossRef](#)]
32. Homaeigohar, S.; Tsai, T.-Y.; Zarie, E.S.; Elbahri, M.; Young, T.-H.; Boccaccini, A.R. Bovine Serum Albumin (BSA)/polyacrylonitrile (PAN) biohybrid nanofibers coated with a biomineralized calcium deficient hydroxyapatite (HA) shell for wound dressing. *Mater. Sci. Eng. C* **2020**, *116*, 111248. [[CrossRef](#)] [[PubMed](#)]
33. Abid, S.; Hussain, T.; Raza, Z.A.; Nazir, A. Current applications of electrospun polymeric nanofibers in cancer therapy. *Mater. Sci. Eng. C* **2019**, *97*, 966–977. [[CrossRef](#)] [[PubMed](#)]
34. Viter, R.; Savchuk, M.; Iatsunskyi, I.; Pietralik, Z.; Starodub, N.; Shpyrka, N.; Ramanaviciene, A.; Ramanavicius, A. Analytical, thermodynamical and kinetic characteristics of photoluminescence immunosensor for the determination of Ochratoxin A. *Biosens. Bioelectron.* **2018**, *99*, 237–243. [[CrossRef](#)] [[PubMed](#)]
35. Fedorenko, V.; Viter, R.; Mrówczyński, R.; Damberg, D.; Coy, E.; Iatsunskyi, I. Synthesis and photoluminescence properties of hybrid 1D core-shell structured nanocomposites based on ZnO/polydopamine. *RSC Adv.* **2020**, *10*, 29751–29758. [[CrossRef](#)]
36. Wang, Z.L. Piezoelectric Nanogenerators Based on Zinc Oxide Nanowire Arrays. *Science* **2006**, *312*, 242–246. [[CrossRef](#)]
37. Ueberschlag, P. PVDF piezoelectric polymer. *Sens. Rev.* **2001**, *21*, 118–126. [[CrossRef](#)]
38. Cui, J.B.; Thomas, M.A. Power dependent photoluminescence of ZnO. *J. Appl. Phys.* **2009**, *106*, 033518. [[CrossRef](#)]
39. Chen, X.-B.; Huso, J.; Morrison, J.L.; Bergman, L. The properties of ZnO photoluminescence at and above room temperature. *J. Appl. Phys.* **2007**, *102*, 116105. [[CrossRef](#)]

**Publisher’s Note:** MDPI stays neutral with regard to jurisdictional claims in published maps and institutional affiliations.



© 2020 by the authors. Licensee MDPI, Basel, Switzerland. This article is an open access article distributed under the terms and conditions of the Creative Commons Attribution (CC BY) license (<http://creativecommons.org/licenses/by/4.0/>).